Inorganic Chemistry
Article
pubs.acs.org/IC

Hydrothermal Preparation and Magnetic Properties of $NaFeSi_2O_6$: Nanowires vs Bulk Samples

Shiliang Zhou,[†] Wolfgang G. Zeier,[†] Moureen C. Kemei,[‡] Moulay T. Sougrati,[§] Matthew Mecklenburg,[∥] and Brent C. Melot*[,†]

[†]Department of Chemistry, University of Southern California, Los Angeles, California 90089, United States
[‡]Materials Department, University of California, Santa Barbara, California 93106-5121, United States
[§]Institut Charles Gerhardt—Laboratoire des Agrégats, Interfaces et Matériaux pour l'Energie, CNRS UMR 5253, 34095 Montpellier Cedex 5, France
[∥]Center for Electron Microscopy and Microanalysis, University of Southern California, Los Angeles, California 90089, United States

Supporting Information

ABSTRACT: A single-step hydrothermal route to the preparation of the pyroxene mineral, $NaFeSi_2O_6$, is reported. The as-prepared samples are found to adopt a nanowire morphology and can be made with a yield of several hundred milligrams at a time with high purity. Synchrotron X-ray diffraction, electron microscopy, and Mössbauer spectroscopy are employed to characterize the structure and morphology. A comparison of the temperature- and field-dependent magnetic properties between the nanowire and sintered phases shows substantial differences that can likely be attributed to the reduced particle size and increased number of spins on the surface of the nanowires.

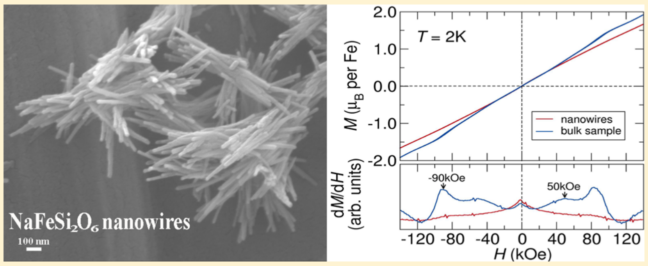

INTRODUCTION

Single-phase materials that simultaneously possess two or more of the primary ferroic properties (ferroelectricity, ferromagnetism, and ferroelasticity), known as multiferroics, have attracted a significant amount of attention due to the coupling that exists between these order parameters.[1] Recently, Jodlauk et al. reported the observation of magnetoelectric coupling in the naturally occurring minerals $NaFeSi_2O_6$.[2] These measurements were conducted on mineral samples, which present some challenges due to compositional inhomogeneities. The single crystals studied by Jodlauk et al. were found to have an average composition determined from electron microprobe analysis of $Na_{1.04}Fe_{0.83}Ca_{0.04}Mn_{0.02}Al_{0.01}Ti_{0.08}Si_2O_6$. While this off-stoichiometry makes an accurate characterization of the magnetic properties difficult, the presence of Mn impurities is guaranteed to alter the nature of the bulk magnetic properties.

The use of mineral samples, instead of phase-pure synthetic samples, is justified by the extreme challenge of preparing phase-pure $NaFeSi_2O_6$. Traditional synthetic routes involve quenching a molten glass with the correct ratio of $Na_2O-Fe_2O_3-SiO_2$ to yield a polycrystalline powder that is then annealed to improve crystallinity and site order.[3] This process can produce nominally pure samples; however, the phase diagram reported by Bowen and co-workers[4] shows that $NaFeSi_2O_6$ melts incongruently above 990 °C, which results in the creation of small impurities of Fe_2O_3 if not cooled quickly enough. More recently, Redhammer et al. reported a method for growing small phase-pure single crystals from fluxes of molten molybdate and vanadate salts.[5] Low temperature neutron diffraction measurements on these single crystals confirmed the existence of complex noncollinear magnetic order in the homogeneous samples, and this is proposed by the authors to be the origin of the magnetoelectric coupling.[5]

Here, we present a route for the preparation of phase-pure polycrystalline $NaFeSi_2O_6$ at low temperatures and pressures. Through a simple digestion of small particles of silica in a strongly basic medium in the presence of a soluble iron salt, we were able to prepare hundreds of milligrams of $NaFeSi_2O_6$ at a time. Electron microscopy showed the powders prepared in this way adopt a wire-like morphology, having widths on the order of a few nanometers. Considering the interest in the multiferroic nature of $NaFeSi_2O_6$, we set out to compare the magnetic properties of these nanowires with the bulk properties. Herein, we show high resolution synchrotron X-ray diffraction, scanning and transmission electron microscopy, Mössbauer spectroscopy, and temperature- and field-dependent magnetization and dielectric measurements which demonstrate that the phase which adopts a nanowire morphology has distinctly different magnetic properties. We attribute the difference in properties to the increased number of iron sites at the surface, which alters the nature of the long-range magnetic order at the transition temperature.

Received: July 18, 2014
Published: November 11, 2014

dx.doi.org/10.1021/ic501664x | *Inorg. Chem.* 2014, 53, 12396−12401

EXPERIMENTAL SECTION

In a typical hydrothermal synthesis, 0.02 mol of NaOH (≥98%, anhydrous pellets, Sigma-Aldrich), 0.01 mol of SiO_2 (fumed silica, 0.2−0.3 μm average particle size, Sigma-Aldrich), and 0.004 mol of $Fe(NO_3)_3{\cdot}9H_2O$ (≥98%, Sigma-Aldrich) were dissolved in 15 mL of deionized water by the order indicated. Then the mixture was transferred into a Teflon-lined stainless steel autoclave, sealed, and maintained at temperatures ranging from 160 to 220 °C for 14 h. After cooling in the air to room temperature, the resulting product was collected and cleaned by filtration with distilled water and ethanol.

In order to prepare bulk samples for the comparison of magnetic properties, the as-prepared powder was pressed into a pellet and heated to 950 °C at a rate of 5 °C/min, held for 40 h, and allowed to cool to room temperature naturally. The bottom of the crucible was lined with powder of the same composition as the pellet to avoid any reactions with alumina.

High resolution synchrotron powder diffraction data were collected using beamline 11-BM at the Advanced Photon Source (APS), Argonne National Laboratory using an average wavelength of 0.413961 Å. Discrete detectors covering an angular range from −6 to 16° 2θ are scanned over a 34° 2θ range, with data points collected every 0.001° 2θ and a scan speed of 0.01° s^{-1}. The resulting diffraction patterns were refined using the Rietveld method with the FullProf program,[6,7] starting with the atomic coordinates determined by Clark et al.[8]

^{57}Fe Mössbauer spectra were measured in the transmission geometry with a source of ^{57}Co in rhodium metal. During the measurements, both the source and the absorber were kept at ambient temperature (294 K). The spectrometer was operated with a triangular velocity waveform. The velocity scale was calibrated with the magnetically split sextet spectrum of a high-purity α-Fe foil as the reference absorber. The absorbers were made by mixing 20 mg of the compound with 80 mg of boron nitride. The spectra of the measured samples were fitted to an appropriate combination of Lorentzian profiles representing quadrupole doublets by least-squares methods. In this way, spectral parameters such as quadrupole splitting (Δ), isomer shift (δ), and relative resonance areas of the different spectral components were determined. Isomer shifts are given relative to α-Fe metal.

Simultaneous Thermogravimetric Analysis (TGA) and Differential Scanning Calorimetry (DSC) measurements were carried out in the temperature range of 30−1100 °C in air the using a Simultaneous Thermal Analyzer (STA-449 Jupiter, Netzsch).

Scanning Electron Microscopy (SEM) was performed on a JEOL JSM-7001 microscope (JEOL Ltd.). Transmission Electron Microscopy (TEM) images were obtained with a JEOL JEM-2100F (JEOL Ltd.) operating at 200 kV. Specimens for TEM were prepared by dispersing the as-prepared sample in ethanol and sonicated for 20 min and then deposited on a 200 mesh Cu grid coated with a Lacey carbon film (Ted Pella, Inc.).

Temperature- and field-dependent magnetic susceptibility and specific heat measurements were collected using a 14 T Quantum Design Dynacool Physical Properties Measurement System. Samples for specific heat measurements were made by mixing the title phase with equal parts by mass of silver powder and pressing into a bar in order to improve thermal coupling to the stage. The specific heat of Ag was measured separately and subtracted.

Capacitance measurements were collected at various frequencies as a function of field and temperature using an Andeen-Hagerling AH2700A capacitance bridge. A 9 T Quantum Design Dynacool Physical Properties Measurement System was used to provide the variable temperature and field environment for capacitance measurements. Prior to measurement, the as-prepared powder was densified using spark plasma sintering with a final density that was 89% of the theoretical maximum. The resulting pellet had a diameter of 10.63 mm and a height of 1.191 mm and was subsequently coated with conducting epoxy to electrically connect the sample to the capacitance probe. Shielded coaxial cables linked the clamped pellet to the capacitance bridge to restrict sample movement during the measurement.

RESULTS AND DISCUSSION

$NaFeSi_2O_6$, commonly known as the mineral aegirine, crystallizes in the $C2/c$ space group. The structure, as illustrated in Figure 1, contains chains of the edge-sharing FeO_6 octahedra which zigzag along the c axis. The FeO_6 chains are connected by the SiO_4 tetrahedra, which form zigzag corner-sharing chains along the c axis (Figure 1b), through sharing the oxygen ions on their edges. Alternatively, the structure can be considered to be formed from close packed Si_2O_6 chains, with Na and Fe ions occupying the octahedral sites (Figure 1a). The interstices, enclosed by the sodium and oxygen atoms, are connected along the c axis and form tunnels with dimensions of 3 Å × 4.4 Å.

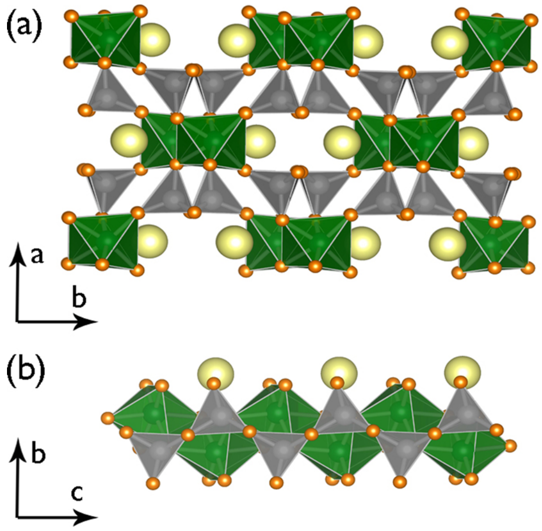

Figure 1. Crystal structure of C 2/c $NaFeSi_2O_6$. The SiO_4 tetrahedra are gray, and the FeO_6 octahedra are green. The sodium and oxygen atoms are shown as yellow and orange spheres, respectively. (a) Close packing Si_2O_6 layered structure with sodium and iron ions located in the octahedral sites. (b) Zigzag edge-sharing FeO_6 chains connected by the zigzag corner-sharing SiO_4 chains through the oxygen ions on their edges.

$NaFeSi_2O_6$ is typically prepared using traditional ceramic reactions or fluxes to grow single crystals, which inevitably require temperatures above 1000 °C, and sometimes high pressure environments.[5,9−12] A relatively low temperature process was reported by Redhammer et al., in which gels were prepared starting from Na_2CO_3, $Fe(NO_3)_3{\cdot}9H_2O$, and TEOS with oxygen fugacity controlled by the pressure vessels, and subsequently heated at temperatures around 700 °C.[13] A similar preparation, reported earlier by Rusakov et al., involved the evaporation of a mixture of $NaNO_3$, $Fe(NO_3)_3$, and silicoethyl ether in ethanol and nitric acid to obtain a gel, which was subsequently annealed at 500 °C and reacted with NaOH solution in Teflon capsules to attain the crystallization of $NaFeSi_2O_6$.[10]

Previous studies of $NaFeSi_2O_6$ have primarily focused on its structural,[8,11−18] spectroscopic,[19,20] and mineralogical properties.[21−23] However, the discovery of multiferroic coupling in the pyroxene $NaFeSi_2O_6$ by Jodlauk et al. led to intensive studies on the magnetic and dielectric properties of $NaFeSi_2O_6$ and similar structures.[2,5,24,25]

The diffraction patterns for powder prepared using the hydrothermal reactions described in the Experimental Section are illustrated in Figure 2. Reactions were carried out from 160 to 220 °C with samples collected at 160 and 170 °C, yielding a red powder while all others were a pale yellow-green. The low temperature samples were found to contain a small amount of hematite mixed with an amorphous phase, indicating a minimum temperature of 180 °C is required to crystallize $NaFeSi_2O_6$. All peaks in the patterns for samples prepared from 180 °C up were found to be fully indexed to the structure reported by Clark et al.[8] Increasing the temperature to 200 °C was found to increase the sharpness of the diffraction peaks, which is likely associated with an increase in particle size. No significant difference in crystallinity or morphology was found between samples prepared at 200 and 220 °C. Hereafter, we refer to the hydrothermal samples prepared at 220 °C as the as-prepared sample when compared to sintered samples.

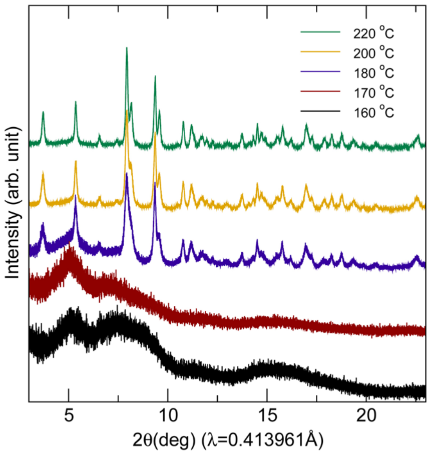

Figure 2. Synchrotron diffraction pattern of products from hydrothermal preparation at temperatures ranging from 160 to 220 °C. A minimum temperature of 180 °C is required to obtain crystalline $NaFeSi_2O_6$.

It is important to note the difference in color between the two temperature regimes. Usually Fe(III) compounds are light yellow to an orangish red. As a point of comparison to the hydrothermal samples, we attempted to prepare $NaFeSi_2O_6$ using a traditional ceramic reaction between oxides and carbonates. Regardless of reaction times or temperatures, a small percentage of hematite impurity was always found and resulted in a completely red product as illustrated in Supporting Information (SI) Figure S1. Previous studies focusing on the solid solution of $NaFeSi_2O_6$ with other minerals and the synthetic $NaFeSi_2O_6$ studied in previous works have reported red coloration.[4,26] The hydrothermally prepared powder is yellowish green, which darkens to an olive green on sintering, which is in good agreement with the coloration of single crystals of $NaFeSi_2O_6$.[11,27]

The morphology of the as-prepared sample was studied by Scanning and Transmission Microscopy, which shows the as-prepared powder consists of $NaFeSi_2O_6$ nanowires that cluster together (Figure 3). The spacing of the lattice fringes indicates that the nanowires predominantly grow along the *c* axis. The wires appear to grow from a common origin and are not simply agglomerated together, so postsynthetic sonication was unable to separate the bundles.

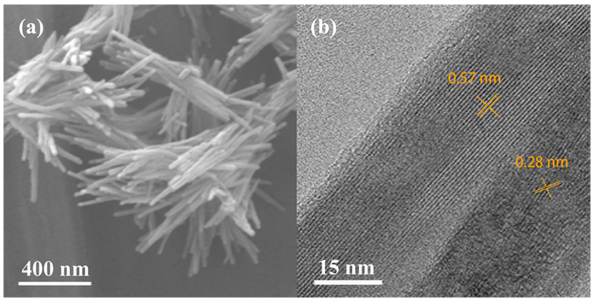

Figure 3. (a) SEM image of the as-prepared $NaFeSi_2O_6$, which is shown to consist of bundles of nanowires. (b) TEM image of the as-prepared sample reveals its crystallinity.

As this is the first nanoscale preparation of $NaFeSi_2O_6$, a comparison with the bulk physical properties is of great interest. Given the difficulties associated with the conventional preparation as previously mentioned, bulk $NaFeSi_2O_6$ was prepared by sintering the as-prepared sample by pressing the powder into a pellet and firing at 950 °C for 40 h. The diffraction pattern of the sintered sample, illustrated in Figure 4, clearly shows significantly sharper peaks, which reflects the substantially increased particle size on firing at elevated temperatures.

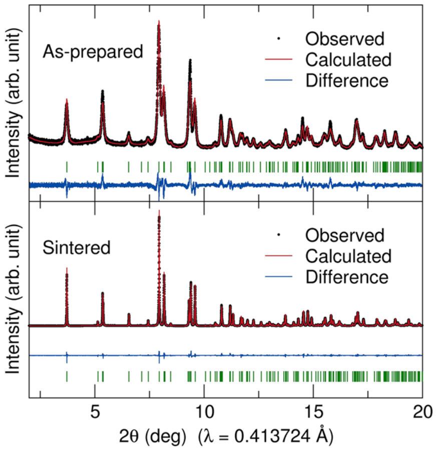

Figure 4. Rietveld refinement of as-prepared and sintered $NaFeSi_2O_6$ against synchrotron X-ray diffraction patterns obtained on the 11-BM beamline at Argonne National Laboratory. χ^2 values of 2.42 and 2.28 for the refinements on the as-prepared sample and the sintered sample were obtained, respectively.

The nanoscale morphology presents some difficulty in refinement of the diffraction pattern. Nevertheless, high-quality fits were achieved for both the as-prepared nanowires prepared at 220 °C and the sintered sample against the high-resolution diffraction data from 11-BM synchrotron facility. However, attempts to refine the atomic displacement parameters (ADP) of the oxygen atoms were tried without any success, which is probably due to the low scattering form factor of oxygen and statistical error. Thus, for the consistency and legitimacy of the refinements, the ADPs of all oxygen atoms are locked at a reasonable value (B_{iso} = 0.3 Å^2). The refinement results are shown in Figure 4. Detailed structural parameters including cell parameters, atomic positions, and atomic displacement parameters are given in SI Tables S1 and S2.

The Mössbauer spectra of the two powders obtained at room temperature are given in Figure 5. The first observation is that for both powders all the iron is in the Fe^{3+} state and no trace of Fe^{2+} is detected. The best fit to the experimental data is obtained using a single doublet (red) for the sintered powder and two doublets (red and blue) for the as-prepared one. This implies that there is only a single type of iron environment with little to no disorder or defects in the sintered powder. In contrast, the need for two doublets as well as the broadening of the spectrum of the as prepared powder indicates that there is a distribution of environments in the as-prepared $NaFeSi_2O_6$. Possible origins for the additional sites could be the presence of an impurity phase (13%, Fe^{3+}) or a sufficient number of defects that a second signal can be seen. Given that no impurity is seen in the synchrotron diffraction data and that the sintered phase, which is made from the as-prepared material, shows no indication of a secondary phases, it is unlikely that an impurity phase is present. The fitted Mössbauer parameters are similar to those reported by Schmidbauer and Kunzmann[20] (note these authors worked at 84 K, which is why they found a higher isomer shift). For the sintered sample, it is extremely well crystallized $NaFeSi_2O_6$. No trace of Fe^{2+} is detected. We thus attribute the additional Fe^{3+} environment in the as-prepared $NaFeSi_2O_6$ to the fact that its surface is hydroxide terminated. Such a finding is fairly reasonable considering the preparation is carried out in aqueous medium and is supported by the presence of hydroxyl stretches in the Raman patterns as well as by a small mass loss in the thermal gravimetric analysis (see SI Figures S2 and S3). The hydroxide terminated surface would also explain that the quadrupole splitting is in close agreement with what is found in hydroxysulfate-based phases.[28]

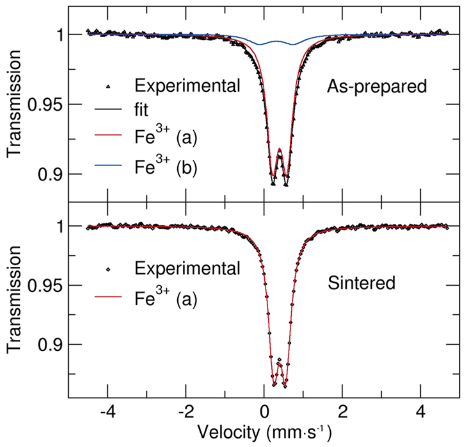

Figure 5. Comparison of the room temperature Mössbauer patterns for the as-prepared and sintered phases. Best fits to the experimental data are obtained with two doublets for the as-prepared sample powder and a single doublet for the sintered one.

Figure 6a shows the temperature-dependent magnetic susceptibility of the as-prepared nanowires in comparison with the phase-pure sintered powders collected from 2 to 300 K in a field of 10 kOe. At first glance, the sintered phase appears to order substantially higher than the as-prepared phase. However, a closer examination of $d\chi/dT$ for the two measurements reveals a single maximum in each sample at 6 and 7 K for the as-prepared and sintered phases, respectively, so there is very little difference in the ordering temperature between the two samples (SI Figure S6). Regardless, there is a clear change in the nature of the ordering since the sintered phase demonstrates the characteristic cusp of an antiferromagnet, whereas the as-prepared powder shows a slight increase in the susceptibility on ordering. We note that the magnetic susceptibility measurements of both samples show no evidence for 8 K transition reported in the natural samples of Jodlauk et al.[2]

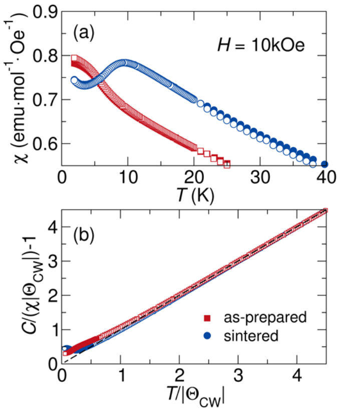

Figure 6. Comparison of the temperature-dependent magnetic susceptibilty for the as-prepared and sintered phases.

To gain more insight into the nature of these differences, the high temperature region (100−400 K) of both measurements was fitted to the Curie−Weiss equation, $C/(T - \Theta_{CW})$ with Curie−Weiss temperatures (effective paramagnetic moments) of −33 K (5.47 μ_B) and −39 K (5.87 μ_B) being found for the as-prepared and sintered phases, respectively. A 4% weight loss found in the TGA analysis of the as-prepared sample was taken into account when normalizing the effective moments for the nanoscale phase. The theoretical spin-only effective moment for a d^5, $S = 5/2$, ion in an octahedral crystal field is 5.92 μ_B, which can be obtained using the relationship $\mu_s = 2(S(S + 1))^{1/2}$. The high temperature data were also fitted using two modifications to the Curie−Weiss equation which incorporated a temperature independent correction, χ_0, and a term to account for noninteracting spins, C/T. A diamagnetic contribution is commonly applied to account for the background from the plastic sample holder, while the noninteracting term has previously been used to model substituted materials where two regions of spins exist.[29] In this instance, the noninteracting term is intended to model disordered spins on the surface of the nanowires. While the addition of the temperature independent term, which typically yielded χ_0 around -4×10^{-4}, resulted in a slight improvement of the fit, the noninteracting term did not appear to improve the quality of the analysis. Thus, despite the increased surface area and the presence of hydroxyl groups in the as-prepared materials, it appears that all of the spins in the materials still experience the same mean field interaction strength. It should also be noted that our results for the sintered sample agree well with the bulk sample studied by Redhammer et al., in which temperature-dependent magnetic susceptibility and neutron diffraction of a $NaFeSi_2O_6$ sample diluted with small amount of SiO_2 and Fe_2O_3 were reported.[5]

Normalizing the inverse susceptibility data to the fitted Curie−Weiss parameters allows a more direct comparison of the temperature-dependent behavior of the two materials. Deviations from ideal Curie−Weiss behavior in such a plot reflect the development of short-range correlations which are antiferromagnetic in the upward direction and ferromagnetic in the negative direction.[30] As seen in Figure 6b, both materials are well described by the Curie–Weiss law until very near theoretical Curie–Weiss ordering temperature ($T/|\Theta_{CW}| = 1$ in this plot), at which point antiferromagnetic correlations begin to develop as expected from the negative sign of the Curie–Weiss theta. This comparison indicates that, despite the jump in the susceptibility on ordering, the overall sign of any short-range correlations in the as-prepared phase is antiferromagnetic, and there is no evidence for ferro- or ferrimagnetic behavior as a function of temperature.

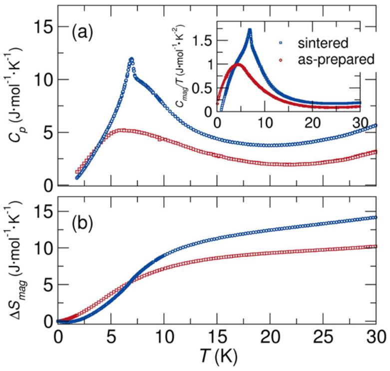

Figure 7. Comparison of the specific heat capacity (a) and change in entropy associated with the magnetic ordering transition (b) for the as-prepared and sintered phases. To obtain more accurate estimation of ΔS_{mag}, the temperature was extrapolated to 0 K by fitting obtained specific heat capacity data in the region of 1.8 to 5 K with a three-parameter polynomial.

Figure 7a shows the temperature-dependent specific heat of the title phases. The horizontal axis was extrapolated to 0 K by fitting data in the region of 1.8 to 5 K with a three-parameter polynomial. Substantial differences can be seen between the two materials, with a sharp lambda-like anomaly that is typically associated with the development of long-range order clearly seen in the sintered material yet absent from the as-prepared powder. Subtracting the lattice contribution and integrating C_p/T yields a change in entropy due to magnetic ordering of 14.2 J·mol^{-1}·K^{-1} for the sintered sample and 10.2 J·mol^{-1}·K^{-1} for the as-prepared sample. The former value is very close to the value of 14.9 J·mol^{-1}·K^{-1} predicted by the Boltzmann equation ($\Delta S = R \ln(2S + 1)$, $S = 5/2$).[31] Lower spin entropy in the as-prepared nanowire sample could be an overestimation of the lattice contribution or the hydroxyls disrupting the spins on the surface of the nanowires. Both values are notably different from those reported in the previous literature, where a value of 11.2 J·mol^{-1}·K^{-1} for a synthetic sample and 13.9 J·mol^{-1}·K^{-1} for a natural sample,[3] as well as 10.5 J·mol^{-1}·K^{-1} for a synthetic sample, were reported.[32]

While the differences in entropy values may simply be due to inaccuracies associated with the estimation of the lattice contribution to the specific heat and other artifacts, a comparison between the overall shapes of the curves should reveal more information about the nature of the materials. C_{mag}/T, where C_{mag} is the magnetic contribution of the specific heat and T is temperature, is plotted against T in the onset of Figure 7a. The broad feature of the as-prepared sample indicates less order in the nanowires, which has been shown in Figure 6. The curve for the sintered sample is highlighted by an ordering peak sitting on a broad hump, which looks very close to that of the synthetic sample reported by Baker et al. and differs significantly from their natural sample.[3] According to Fisher, the heat capacity of an antiferromagnet can be determined from the magnetic susceptibility by using the equation $C_{(T)} = A(\partial(\chi T)/\partial T)$.[33] A comparison between the Fisher heat capacity (SI Figure S7) and specific heat curve of the sintered material reveals that the broad hump is probably responsible for the spin entropy, while the leading feature could be associated with the 8 K transition that we do not detect in temperature dependent susceptibility measurements (Figure 6 and SI Figure S6). The origin of these transitions has been discussed in previous literature,[2,3] and an accurate probe would require more advanced experiments such as low-temperature neutron scattering, which are beyond the scope of this report.

Figure 8a shows the constant temperature magnetization loops at 2 K. The as-prepared material shows a nearly linear response to the application of a strong magnetic field, as would be expected for an antiferromagnetically ordered material; however, there is clearly a slight curvature. In contrast, the sintered material shows two distinct field-induced features in the magnetization at ±50 kOe and ±90 kOe as emphasized in Figure 8b. These field-induced features may be related to the reorientation of the ferrolectric polarization from the b axis to the c axis that was reported in the work of Jodlauk et al.[2] In contrast to what was found there, our measurements show that the field-induced change in the dielectric properties does not occur until significantly higher fields than previously observed in the site-mixed geological samples. Constant temperature loops of sintered $NaFeSi_2O_6$ at temperatures from 3 to 8 K can be found in SI Figure S8a. The derivative curves, shown in Figure S8b, indicate only one of these field-induced features persists at temperatures from 3 to 7 K, and both of them are absent at temperatures above 7 K.

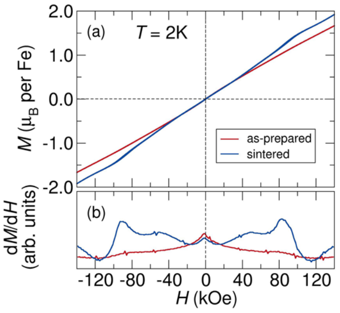

Figure 8. Comparison of the constant temperature magnetization loops for the as-prepared and sintered $NaFeSi_2O_6$ at 2 K. The magnetization of the as-prepared $NaFeSi_2O_6$ nanowires shows a nearly linear response to the applied magnetic field, while two distinct field-induced features are observed in the sintered sample.

In order to examine whether this field-induced feature was really correlated with changes in the electric polarization, magnetocapacitance measurements were collected on a densified pellet of the sintered phase. Since capacitance measurements require a highly dense pellet, it was not possible to measure the capacitance of the as-prepared nanowires for comparison. Field- and temperature-dependent capacitance measurements of $NaFeSi_2O_6$ are illustrated in SI Figures S4 and S5, respectively. We observe a jump in the dielectric constant at 7 K, compared to a value of 6 K paraelectric to ferroelectric transition reported by Jodlauk et al.[2] While the ferroelectric transition is field-dependent according to the report of Jodlauk et al., our results show a constant transition temperature (T_{FE})

in varying fields (SI Figure S5). Above T_{FE}, the capacitance is field-independent (SI Figure S4a); however, significant enhancement of the capacitance is observed in what Jodlauk et al. identified as a ferroelectric phase when 60 kOe ≤ H ≤ 80 kOe. However, the use of powder samples in our measurements restricts our results to average bulk properties. Fully resolving the orientation-dependent magnetic and dielectric properties would require the preparation of high-purity single crystals.

■ CONCLUSION

We present a single-step route for the preparation of phase-pure nanowires of $NaFeSi_2O_6$ at low temperatures and pressures. Considering the interest in the multiferroic nature of $NaFeSi_2O_6$, we set out to compare the magnetic properties of these nanowires with sintered bulk samples. Herein, we show high resolution synchrotron X-ray diffraction, scanning and transmission electron microscopy, Mössbauer spectroscopy, and temperature- and field-dependent magnetization measurements which demonstrate that the phase that adopts a nanowire morphology has distinctly different magnetic properties from the bulk sample. We attribute the difference in properties to the increased number of iron sites at the surface, which alters the nature of the long-range magnetic order at the transition temperature.

■ ASSOCIATED CONTENT

Ⓢ Supporting Information

This material is available free of charge via the Internet at http://pubs.acs.org.

■ AUTHOR INFORMATION

Corresponding Author

*E-mail: melot@usc.edu.

Notes

The authors declare no competing financial interest.

■ ACKNOWLEDGMENTS

The authors acknowledge financial support through start-up funding provided by the Dana and David Dornsife College of Letters, Arts and Sciences at the University of Southern California. This project was supported by the NSF through the DMR 1105301. M.C.K. is supported by the Schlumberger Foundation Faculty for the Future fellowship. We acknowledge the use of MRL Central Facilities which are supported by the MRSEC Program of the NSF under Award No. DMR 1121053, a member of the NSF-funded Materials Research Facilities Network (www.mrfn.org). Use of the Advanced Photon Source at Argonne National Laboratory was supported by the U.S. Department of Energy, Office of Science, Office of Basic Energy Sciences, under Contract No. DE-AC02-06CH11357.

■ REFERENCES

(1) Eerenstein, W.; Mathur, N. D.; Scott, J. F. *Nature* **2006**, *442*, 759−765.

(2) Jodlauk, S.; Becker, P.; Mydosh, J. A.; Khomskii, D. I.; Lorenz, T.; Streltsov, S. V.; Hezel, D. C.; Bohaty, L. *J. Phys.: Condens. Matter* **2007**, *19*, 432201.

(3) Baker, P. J.; Lewtas, H. J.; Blundell, S. J.; Lancaster, T.; Franke, I.; Hayes, W.; Pratt, F. L.; Bohaty, L.; Becker, P. *Phys. Rev. B* **2010**, *81*, 214403.

(4) Bowen, N.; Schairer, J.; Willems, H. *Am. J. Sci.* **1930**, *20*, 405−455.

(5) Redhammer, G. J.; Senyshyn, A.; Meven, M.; Roth, G.; Prinz, S.; Pachler, A.; Tippelt, G.; Pietzonka, C.; Treutmann, W.; Hoelzel, M.; Pedersen, B.; Amthauer, G. *Phys. Chem. Miner.* **2011**, *38*, 139−157.

(6) Rietveld, H. M. *J. Appl. Crystallogr.* **1969**, *2*, 65.

(7) Rodríguez-Carvajal, J. *Physica B* **1993**, *192*, 55−69.

(8) Clark, J. R.; Appleman, D. E.; Paplike, J. *Mineral. Soc. Am.: Special Papers* **1969**, *2*, 31−50.

(9) Baum, E.; Treutmann, W.; Behruzi, M.; Lottermoser, W.; Amthauer, G. *Z. Kristallogr.* **1988**, *183*, 273−284.

(10) Rusakov, V. S.; Yagova, O. E.; Kuz'mina, N. A.; Bychkov, A. M. *Geokhimiya* **1999**, 404−409.

(11) Redhammer, G. J.; Roth, G. *Z. Kristallogr.* **2002**, *217*, 63−72.

(12) Redhammer, G. J.; Amthauer, G.; Roth, G.; Tippelt, G.; Lottermoser, W. *Am. Mineral.* **2006**, *91*, 1271−1292.

(13) Redhammer, G. J.; Amthauer, G.; Lottermoser, W.; Treutmann, W. *Eur. J. Mineral.* **2000**, *12*, 105−120.

(14) Nolan, J.; Edgar, A. D. *Mineral. Mag.* **1963**, *33*, 625−634.

(15) Nolan, J. *Mineral. Mag.* **1969**, *37*, 216−229.

(16) Consortium Mat Property Res Earth Sci; High Pressure Collaborat AccessEOLEOLTeam; Florida Int Univ, Coll Engn.: Downs, R. T.; Singh, A. K. *J. Phys. Chem. Solids* **2006**, *67*, 1995−2000.

(17) Weigel, C.; Cormier, L.; Galoisy, L.; Calas, G.; Bowron, D.; Beuneu, B. *Appl. Phys. Lett.* **2006**, *89*, 141911.

(18) Redhammer, G. J.; Tippelt, G.; Amthauer, G.; Roth, G. *Z. Kristallogr.* **2012**, *227*, 396−410.

(19) Zhang, M.; Redhammer, G. J.; Salje, E. K. H.; Mookherjee, M. *Phys. Chem. Miner.* **2002**, *29*, 609−616.

(20) Schmidbauer, E.; Kunzmann, T. *Phys. Chem. Miner.* **2004**, *31*, 102−114.

(21) Grew, E. S.; Belakovskiy, D. I.; Fleet, M. E.; Yates, M. G.; Mcgee, J. J.; Marquez, N. *Eur. J. Mineral.* **1993**, *5*, 971−984.

(22) Mcswiggen, P. L.; Morey, G. B.; Cleland, J. M. *Can. Mineral.* **1994**, *32*, 589−598.

(23) Prestvik, T.; Barnes, C. G. *Norw. J. Geol.* **2007**, *87*, 451−456.

(24) Mettout, B.; Toledano, P.; Fiebig, M. *Phys. Rev. B* **2010**, *81*, 214417.

(25) Kim, I.; Jeon, B.-G.; Patil, D.; Patil, S.; Nenert, G.; Kim, K. H. *J. Phys.: Condens. Matter* **2012**, *24*, 306001.

(26) Ballet, O.; Coey, J. M. D.; Fillion, G.; Ghose, A.; Hewat, A.; Regnard, J. R. *Phys. Chem. Miner.* **1989**, *16*, 672−677.

(27) Frondel, C.; Ito, J. *Am. Mineral.* **1966**, *51*, 1406−1413.

(28) Ati, M.; Sougrati, M.-T.; Rousse, G.; Recham, N.; Doublet, M.-L.; Jumas, J.-C.; Tarascon, J.-M. *Chem. Mater.* **2012**, *24*, 1472−1485.

(29) Lawes, G.; Risbud, A. S.; Ramirez, A. P.; Seshadri, R. *Phys. Rev. B* **2005**, *71*, 045201.

(30) Melot, B. C.; Drewes, J. E.; Seshadri, R.; Stoudenmire, E. M.; Ramirez, A. P. *J. Phys.: Condens. Matter* **2009**, *21*, 216007.

(31) Melot, B. C.; Goldman, A.; Darago, L. E.; Furman, J. D.; Rodriguez, E. E.; Seshadri, R. *J. Phys.: Condens. Matter* **2010**, *22*, 506003.

(32) Ko, H. C.; Ferrante, M. J.; Stuve, J. M. *Proceedings of the Seventh Symposium on Thermophysical Properties*; American Society of Mechanical Engineers: New York, 1977; p 392.

(33) Fisher, M. E. *Proc. R. Soc. London Ser. A* **1960**, *254*, 66−85.